Supporting Information

Dual self-trapped exciton emission of $(TBA)_2Cu_2I_4$: optical properties and high anti-water stability

Hui Peng,[a,b,c‡] Yonghao Xiao,[a‡] Ye Tian,[c] Xinxin Wang,[c] Tao Huang,[b] Tiantian Dong,[d] Yueting, Zhao,[d] Jianping Wang,*[d] and Bingsuo Zou*[b]

[a]School of Materials Science & Engineering, Beijing Institute of Technology, Beijing 100081, China.

[b]Guangxi Key Lab of Processing for Nonferrous Metals and Featured Materials and Key Lab of New Processing Technology for Nonferrous Metals and Materials, Ministry of Education; School of Resources, Environments and Materials, Guangxi University, Nanning 530004, China.

[c]Beijing Key Laboratory of Nanophotonics & Ultrafine Optoelectronic Systems, Beijing Institute of Technology, Beijing 100081, China.

[d]Beijing National Laboratory for Molecular Sciences, Institute of Chemistry, Chinese Academy of Sciences, Beijing 100190, China.

*Corresponding Author: E-mail: zoubs@gxu.edu.cn, jwang@iccas.ac.cn

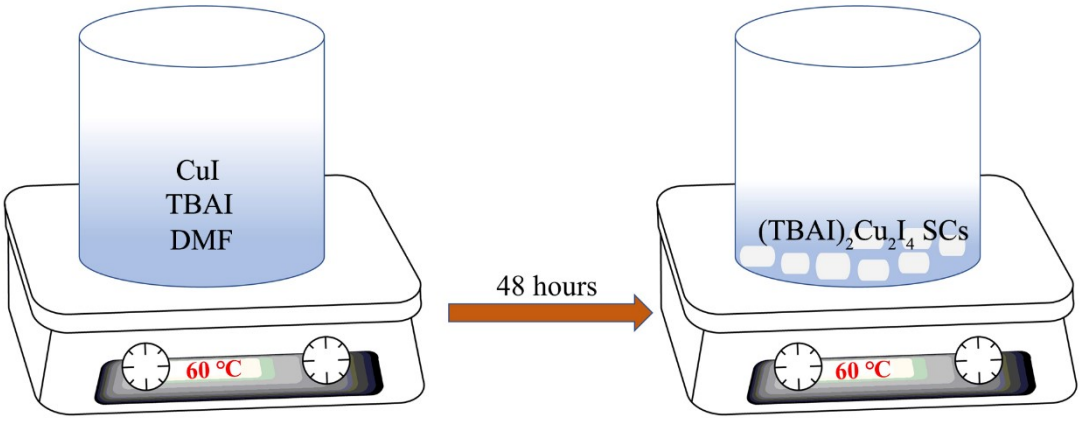

Figure S1. Schematic illustration of synthetic process of $(TBA)_2Cu_2I_4$ SCs by using a slow evaporation technology of solution.

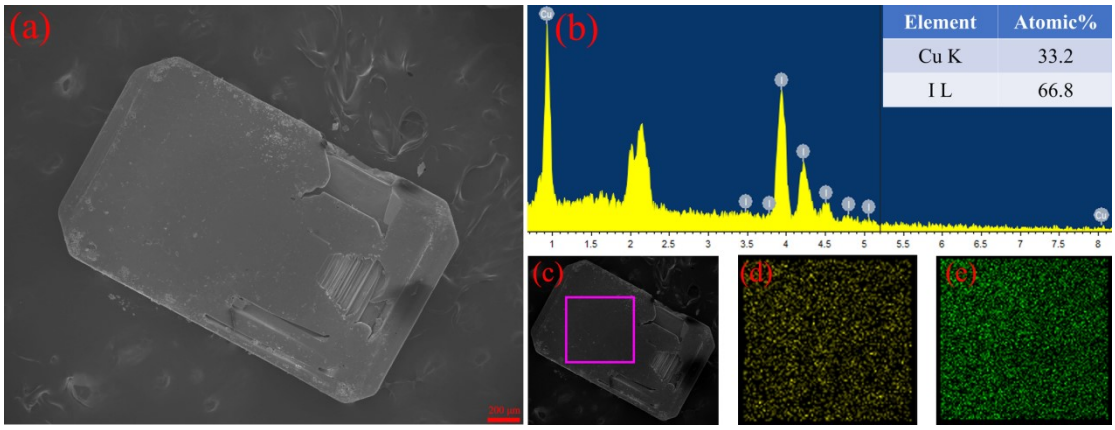

Figure S2. SEM image of $(TBA)_2Cu_2I_4$ SC. (b) Energy dispersive spectrum (EDS) of $(TBA)_2Cu_2I_4$. The inset is the percentage of element content of $(TBA)_2Cu_2I_4$. (c)-(e) Elemental mapping images of $(TBA)_2Cu_2I_4$ for the detected elements: (d) Cu and (e) I.

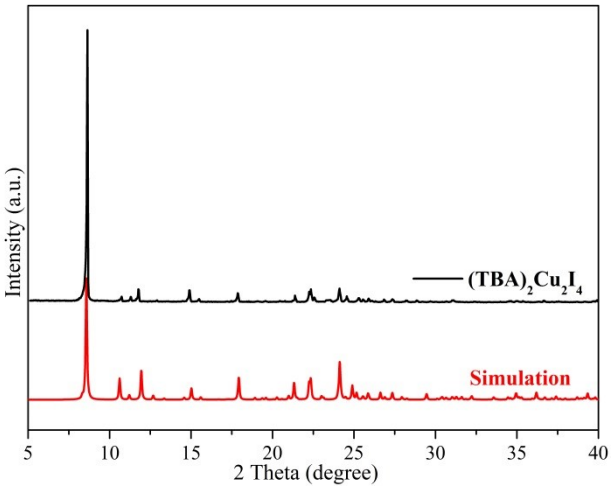

Figure S3. Experimental and simulated PXRD patterns of $(TBA)_2Cu_2I_4$.

Clearly, although the PXRD results show almost identical characteristics with the simulated SCXRD patterns, there is still a slight deviation from the simulated one, which is normal. As we know, the single crystal XRD (SCXRD) is usually different from the PXRD. For the SCXRD, the simulated PXRD results are easily affected by the quality of the crystal, and the tiny defects in the single crystal also affect the results. The experimental PXRD, i.e. polycrystalline diffraction, the results are affected by many factors, such as: the size of polycrystalline powders, crystal orientation, the way of sample tiling, and so on. Moreover, some patterns or peaks may not show up due to the preferred orientation and selection rules of the crystal, this also affect the results. Therefore, the perfect correspondence or consistence between SCXRD and PXRD is an ideal situation, the slight difference between single crystal XRD and PXRD data within a reasonable range is acceptable.

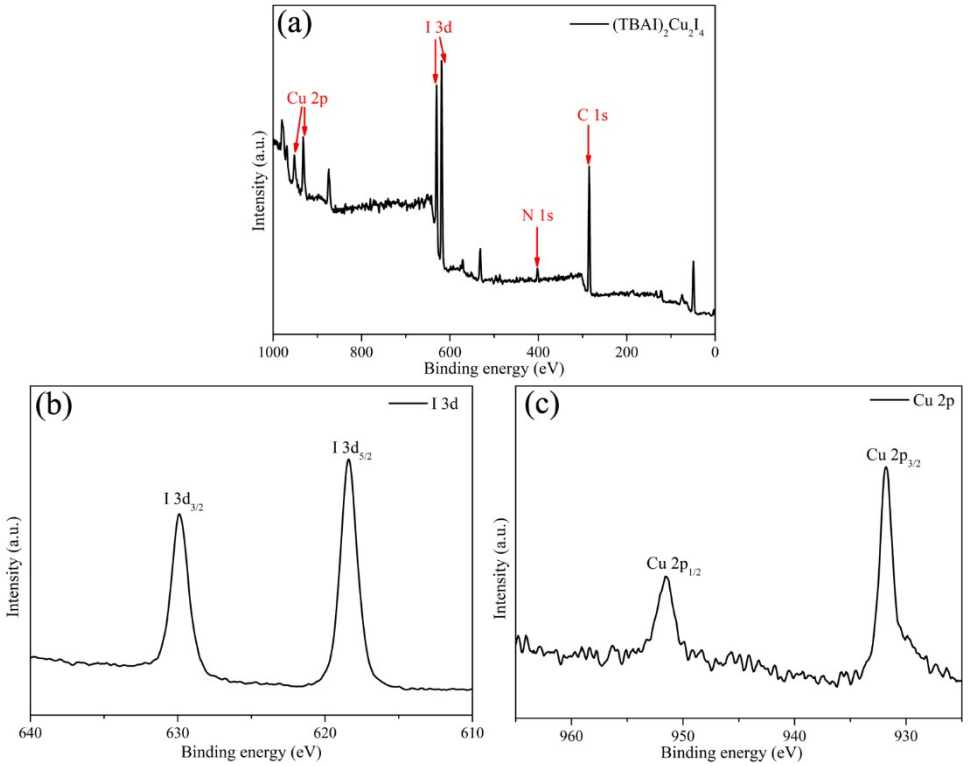

Figure S4. (a) X-ray photoelectron spectroscopic (XPS) analysis of $(TBA)_2Cu_2I_4$ powders and the high-resolution spectra of (b) I 3d and (c) Cu 2p.

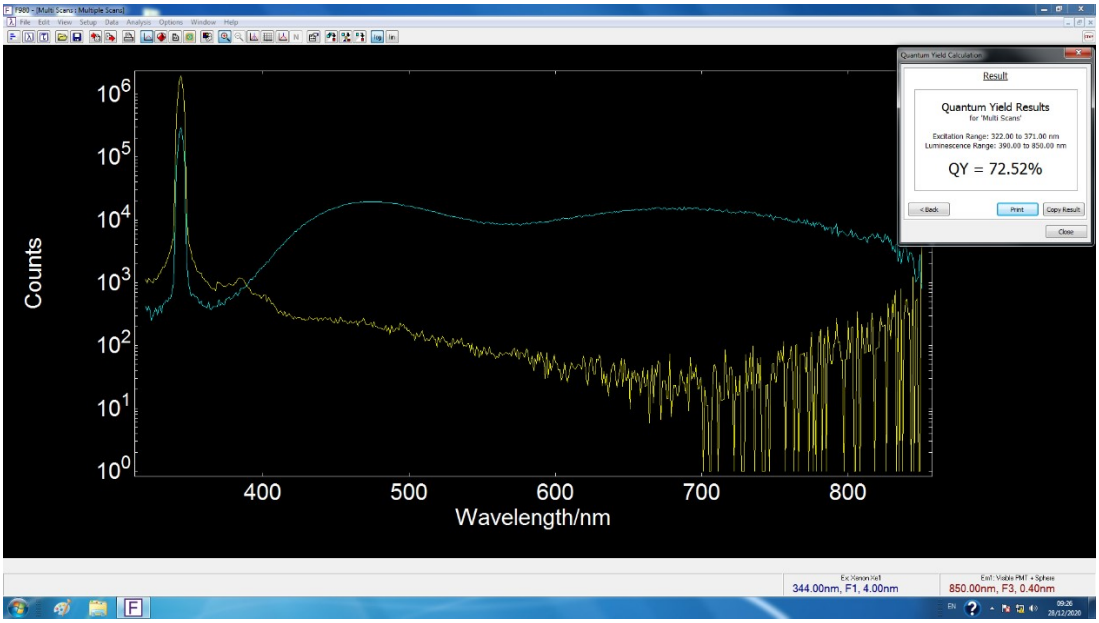

Figure S5. Absolute photoluminescence quantum yield measurement of the $(TBA)_2Cu_2I_4$ single crystals.

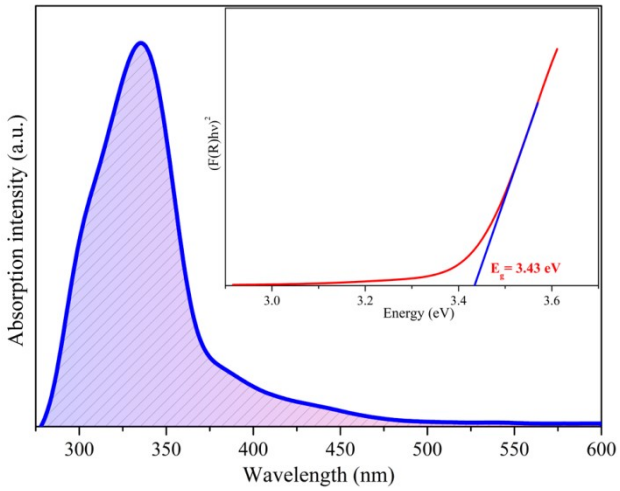

Figure S6. UV−visible absorption spectrum of $(TBA)_2Cu_2I_4$ at room temperature. The inset shows the band gap of $(TBA)_2Cu_2I_4$ determined from a Tauc plot with a band gap of 3.43 eV.

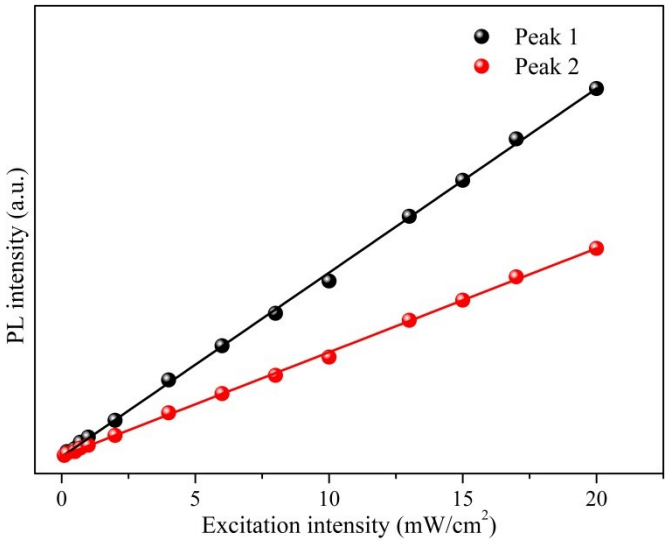

Figure S7. The PL intensity of the dual-emission band versus excitation power for $(TBA)_2Cu_2I_4$ SCs at room temperature.

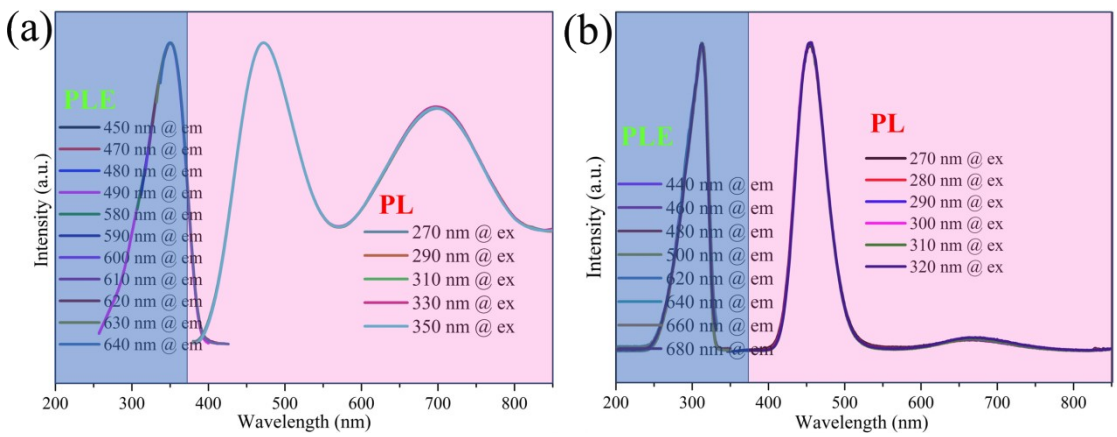

Figure S8. Emission-wavelength-dependent PLE and PL spectra of $(TBA)_2Cu_2I_4$ at 298 K (a) and 78 K (b), respectively.

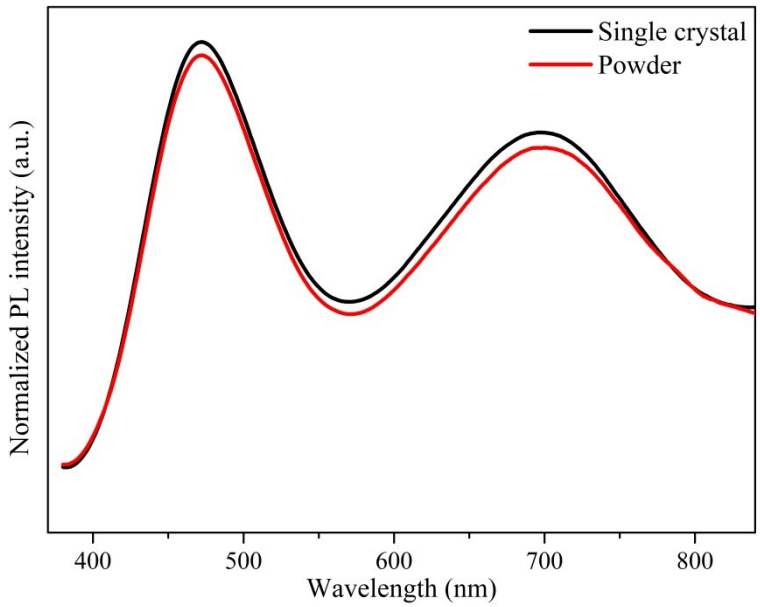

Figure S9. PL spectra of $(TBA)_2Cu_2I_4$ SCs and ball-milled powders measured at room temperature.

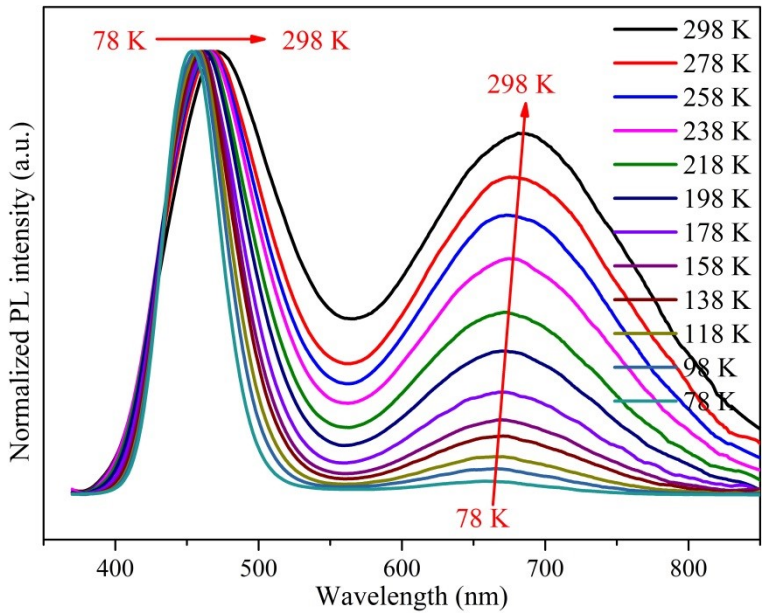

Figure S10. Temperature-dependent PL spectra in the temperature range of 78-298 K.

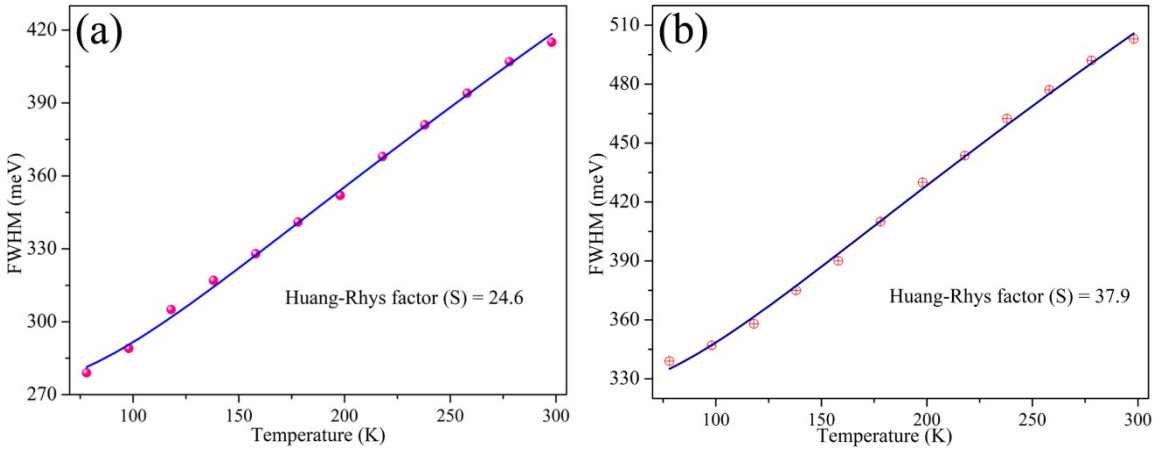

Figure S11. Fitting results of the FWHM (meV) as a function of temperature via the formula of $FWHM = 2.36\sqrt{S}\hbar\omega_{phonon}\sqrt{coth\frac{\hbar\omega_{phonon}}{2K_BT}}$ to obtain the Huang-Rhys factor (S), where ω_{phonon} is the frequency of longitudinal optical (LO) phonon. Clearly, one can calculate that the values of S are 24.6 (peak 1, Figure S11a) and 37.9 (peak 2, Figure S11b).

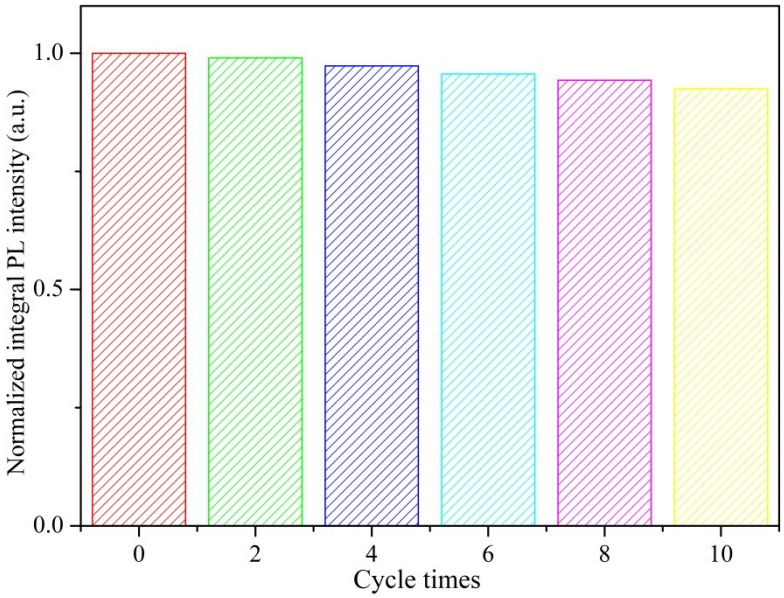

Figure S12. The change of the PL intensity in cyclic test in the temperature range of 78-298 K.

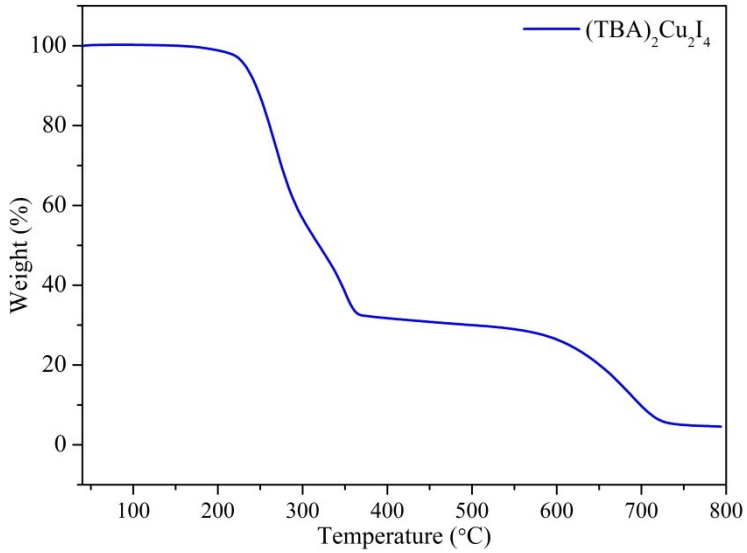

Figure S13. TG curve of $(TBA)_2Cu_2I_4$ powders.

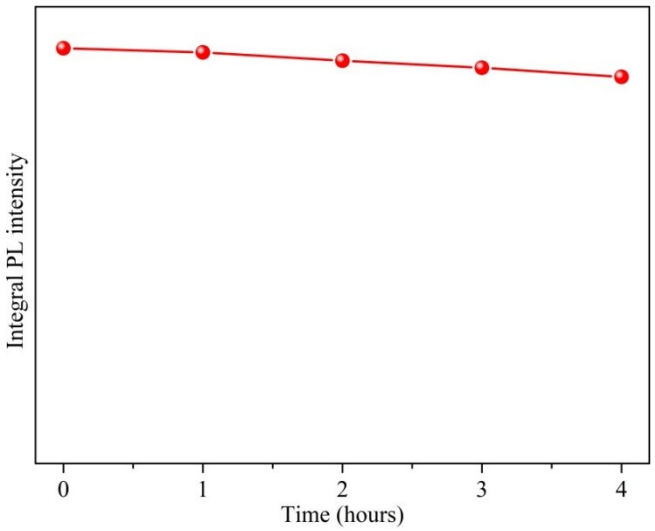

Figure S14. Long-term stability of $(TBA)_2Cu_2I_4$ SCs under a 340 nm UV lamp within 4 hours.

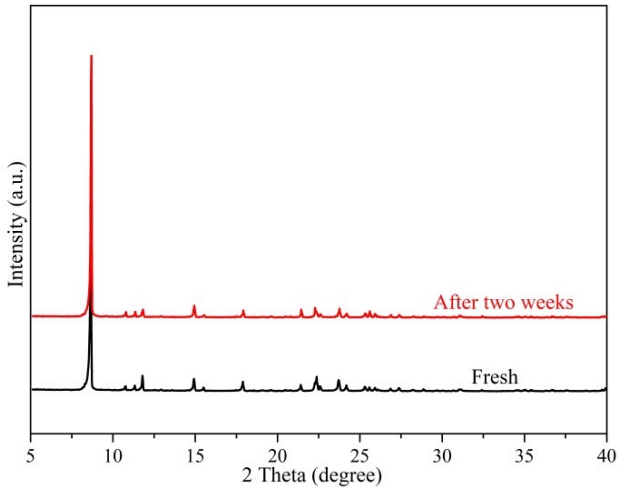

Figure S15. PXRD patterns of $(TBA)_2Cu_2I_4$ before and after exposure to atmospheric environment (～35 % relative humidity) for two weeks.

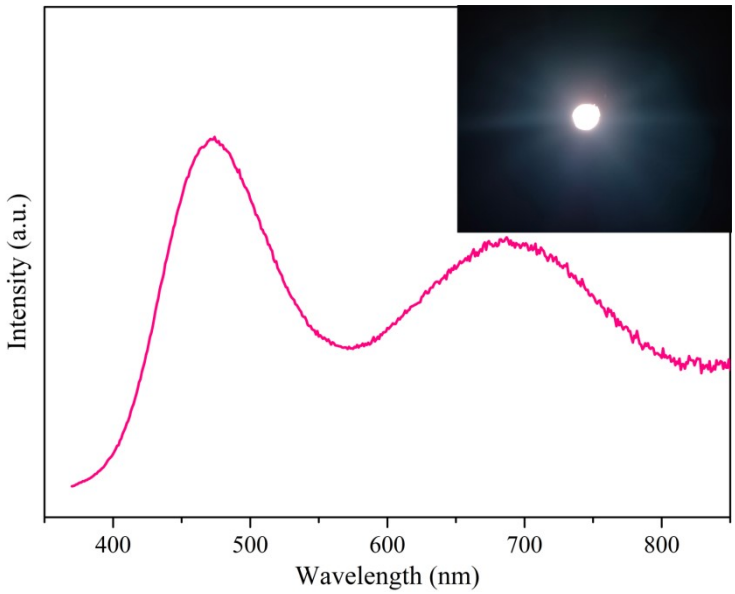

Figure S16. Emission spectrum of a single-compound white-light LED based on $(TBA)_2Cu_2I_4$ powders. The inset image shows a bright white light emission under UV chip excitation.

Table S1. Huang-Rhys factors for different compounds.

Compounds	Huang-Rhys factors (*S*)	Refs.
CdSe	1	1
ZnSe	0.3	2
$CsPbBr_3$	3.2	3